Climatic Change (2019) 153:341–359
https://doi.org/10.1007/s10584-019-02396-8

Changes of East Asian summer monsoon due to tropical air-sea interactions induced by a global warming scenario

Yan Jin[1] · Cristiana Stan[1,2]

Received: 11 June 2018 / Accepted: 18 February 2019 / Published online: 28 February 2019

Abstract
The changes of the East Asian summer monsoon (EASM) in response to increased CO_2 atmospheric forcing are analyzed using the Super-Parameterized Community Climate System Model version 4 (SP-CCSM4). In response to the global warming caused by the increased atmospheric CO_2 concentration, the precipitation and circulation of the EASM intensify. These changes are explained by the westward extension of the western North Pacific subtropical high (WNPSH). The displacement of the WNPSH is caused by two mechanisms: (i) the increase of sea surface temperature and (ii) the reduction of latent heat flux over the South China Sea and adjacent western Pacific Ocean. The changes in the surface fluxes over the tropics induce a Gill-type anticyclonic circulation in the lower troposphere to the north of the heating anomaly and a Rossby wave train from the tropics into the mid-latitude Pacific Ocean. The westerly anomalies on the northern side of the anticyclone strengthen the southwesterly flow on the western edge of the WNPSH. This flow further affects the wind anomalies and moisture transport over East Asia. The Rossby wave train affects the large-scale circulation associated with the WNPSH.

1 Introduction

The East Asian summer monsoon (EASM) is an important component of the global monsoon system (He et al. 2007) and the Asian climate system (Tao and Chen 1987). The EASM is affected by the climatic systems from the tropics, subtropics, and mid-latitudes, which makes it a hybrid tropical-subtropical monsoon system (Ninomiya and Murakami 1987).

Electronic supplementary material The online version of this article (https://doi.org/10.1007/s10584-019-02396-8) contains supplementary material, which is available to authorized users.

✉ Cristiana Stan
cstan@gmu.edu

[1] Department of Atmospheric, Oceanic and Earth Sciences, George Mason University, Fairfax, VA 22030, USA

[2] Center for Ocean-Land-Atmosphere Studies, Fairfax, VA 22030, USA

A number of observational studies analyzing the trend over the recent decades in the EASM rainfall showed a tendency towards increased regional precipitation in central and southern China and droughts in northern and northeastern China (e.g., Menon et al. 2002; Hu et al. 2003; Li et al. 2010).

Numerous studies indicate that in a warmer climate, the EASM mean precipitation will intensify due to an enhancement of monsoon circulation, local water vapor buildup, and moisture transport into the EASM region (e.g., Hu et al. 2003; Kimoto 2005; Kitoh and Uchiyama 2006; Kripalani et al. 2007; Lu et al. 2007; Sun and Ding 2010; Kusunoki and Arakawa 2012). One explanation for the EASM intensification is that as the global temperature rises, an El Niño-like pattern will develop more frequently (Kurihara et al. 2005). This pattern will reduce the sea surface temperature (SST) gradient across the equatorial Pacific Ocean and strengthen the downward airflow over the tropical western Pacific Ocean (the downward branch of the Walker circulation) and intensify the western North Pacific subtropical high (WNPSH). The strengthening of the WNPSH leads to a stronger southwesterly flow, which enhances the moisture transport over East Asia. More recent studies based on the models of phase 3 and phase 5 of the Coupled Model Inter-comparison Project (CMIP3, CMIP5) also found an intensification of the EASM in response to global warming (e.g., Lee and Wang 2014; Chen and Bordoni 2016). Their results indicate that the intensification of the EASM may be attributed to both enhancement and westward displacement of the WNPSH. Besides the intensification of the mean state of the EASM, its variability would also change in a global warming climate (e.g., Kitoh and Uchiyama 2006; Kripalani et al. 2007; Kusunoki and Arakawa 2012). Kripalani et al. (2007) analyzed the response of the EASM to a climate change scenario due to CO_2 doubling simulated by 22 models of IPCC AR4 and found an increase in the mean EASM precipitation and an extension of the rainy season. Kitoh and Uchiyama (2006) showed that the withdrawal of the rainy season over Japan is delayed in a global warming scenario.

Previous work mentioned above generally attributed the changes of the EASM to the enhancement and westward displacement of the WNPSH as well as a stronger moisture transport into East Asia. The strength, shape, and position of the WNPSH are key factors influencing EASM precipitation (e.g., Lu and Dong 2001; Mao et al. 2010; Sun and Ying 1999; Lu 2001; Zhang et al. 2009; Huang and Sun 1992; Yang and Sun 2003; Zhang and Tao 1999; Zhou et al. 2009) and WNPSH links the tropical and extra-tropical circulations driving the EASM variability (Sun and Ying 1999). The low-level jet at the northwestern edge of the WNPSH transports large amounts of moisture into the EASM region and the meridional shifts of the WNPSH have been associated with the onset and retreat of the EASM in observations.

The observed relationship between the EASM and the WNPSH (Ding and Chan 2005) implies that mechanisms explaining changes in the WNPSH in a warmer climate are essential for understanding the variations in the EASM. Li et al. (2012) showed that the intensification of the WNPSH in response to higher greenhouse gas concentrations is primarily caused by enhanced diabatic heating over land and cooling over ocean, which induces an increase in the land-sea thermal contrast. In a warmer climate, the enhanced diabatic heating (cooling) over land (ocean) induces an anticyclonic anomaly over the ocean, leading to the strengthening of the WNPSH. Zhou et al. (2009) found that the westward extension of the WNPSH is related to the Indian Ocean-western Pacific (IWP) warming. The warmer SST over IWP increases precipitation locally and intensifies convective heating. The positive SST anomalies over IWP affect the Walker circulation and lead to deficient precipitation over the central and eastern tropical Pacific Ocean, resulting in a negative heating anomaly there. The negative

heating anomaly induces a baroclinic mode as described in the simple model of Gill (1980), generating one pair of anticyclonic circulations in the western North Pacific (WNP). In addition, the low-level equatorial flank of the WNPSH can be partly interpreted as a Kelvin wave response to the diabatic heating of South Asian monsoon rainfall (Zhou et al. 2009). The warming of IWP induces easterly anomalies to the east of the heat source, which intensifies the easterlies on the equatorial flank of the WNPSH. This mechanism, proposed by Rodwell and Hoskins (1996), plays a secondary role in the westward extension of the WNPSH. However, the increased SST over IWP reduces the land-sea thermal contrast. As pointed out by Li et al. (2012), the reduced land-sea thermal contrast weakens the intensity of the WNPSH.

The air-sea interaction processes affecting the surface fluxes also play a role in the WNPSH variability (Huang et al. 2010; Wang et al. 2013; Xiang et al. 2013). To the southeast of the WNPSH anomaly, the anomalous northeasterlies strengthen the mean easterly wind and thus enhance the evaporation/entrainment, which yields to a cooling of the ocean. The negative SST anomaly suppresses the convective activity, which results in a reduction of the diabatic heating and generation of anticyclonic vorticity to the north of cold SST (Gill-type). Thus, the ocean cooling further enhances the WNPSH anomaly. Also, to the southwest of the WNPSH, the easterly anomaly weakens the mean southwesterly flow and warms the northern Indian Ocean (IO). The warming of IO induces Kelvin waves to its east and favors the WNPSH enhancement.

According to the mechanisms mentioned above, the EASM changes in a warmer climate are closely related to the variations in the WNPSH, which are attributed to the changes in the mean state of the boundary conditions (Zhou et al. 2009; Wang et al. 2013; Xiang et al. 2013; Cevuturi et al. 2018). However, the impacts of changes induced by global warming in the South China Sea (SCS) and western Pacific Ocean (WP) onto the EASM are not completely understood. These regions play an important role in moisture transport for EASM precipitation (Ding et al. 2005). Recent studies showed that global warming induces changes in atmospheric heating, low-tropospheric convergence, and sea-level pressure over SCS and WP in boreal summer (He et al. 2016), along with a decrease of boreal spring precipitation over southern China (Li et al. 2016). The goal of this work aims to demonstrate that changes in the local air-sea interaction over SCS and adjacent WP induced by the global warming also have an impact on the displacement of the WNPSH, thus influencing EASM precipitation.

The rest of the paper is organized as follows. Section 2 discusses the EASM response to a global warming scenario associated with an increase in the atmospheric CO_2 concentration based on a suite of climate simulations. These numerical simulations consist of a coupled ocean-atmosphere simulation corresponding to a present-day external forcing, a coupled ocean-atmosphere simulation with abrupt quadrupling of atmospheric CO_2 concentration, and two AMIP-type simulations. The first AMIP simulation uses observed SST as boundary conditions and the atmospheric CO_2 concentration matches that of the global warming coupled simulation. This simulation captures the rapid adjustment of atmosphere to the increase of CO_2 concentration. The second AMIP simulation uses the observed SST + 4K as boundary conditions and the atmospheric CO_2 concentration matches that of the present day coupled simulation. This simulation captures the slow adjustment of atmosphere to the increase of CO_2 concentration through the SST influence. Analysis of these simulations suggest that surface heat fluxes over SCS and WP induced by the global warming explain the changes in EASM precipitation associated with the global warming caused by the quadrupling of atmospheric CO_2. To validate this hypothesis, two more AMIP-type experiments are conducted to establish the sensitivity of EASM precipitation to the remote influence over SCS and WP regions. These

sensitivity-type experiments are discussed in Section 3 along with the mechanisms on how and why changes in the surface heat fluxes over SCS and WP induced by the global warming affect EASM precipitation. Summary and discussions are presented in Section 4.

2 EASM response to global warming

2.1 Model simulations

To test the air-sea interaction hypothesis, four numerical experiments were conducted with the SP-CCSM4 model (Stan and Xu 2014): two ocean-atmosphere coupled runs and two AMIP-type runs. The coupled runs are the present-day control with atmospheric CO_2 concentration of 368.9 ppmv (pdControl) and the coupled global warming scenario with the abrupt quadrupling of atmospheric CO_2 concentration of the pdControl control (cpl_4×CO_2). Both coupled simulations are initialized in 2006 and extend across 150 years. The specifics of these experiments are summarized in Table 1, which provides an overview of all numerical experiments conducted in this study and the description of the model is given in Supplemental. The AMIP-type simulations are defined by the CMIP5 protocol as diagnostic or complimentary experiments to the coupled climate change simulations designed to understand the "fast" and "slower" response to external forcing (Hensen et al. 2005). The first AMIP run uses boundary conditions of observed (1949–2001) mean SST and sea ice datasets (Hurrell et al. 2008) and the same atmospheric CO_2 concentration as in cpl_4×CO2 (amip_4×CO_2). In the second AMIP run (amip_4K), the observed SST is perturbed by a uniform 4K increase with the same atmospheric CO_2 concentration as in the pdControl run. Because the sea ice is not changed in any of the AMIP-type experiments, boundary conditions will refer to SST throughout the paper. The two AMIP-type simulations are also initialized in 2006 and run for 35 years. In the coupled runs, the atmosphere and ocean are fully coupled. The heat, momentum, and moisture are exchanged at the air-sea interface. In the uncoupled runs, the air-sea interaction is cut off and the ocean cannot respond to the atmosphere forcing. Thus, the amip_4×CO_2 run shows only the impact of quadrupling the CO_2 level on the atmosphere (the fast response), whereas the amip_4K run shows the direct effect of SST warming on the atmosphere (the slow response). The complete description of these runs is given by Bretherton et al. (2014), who also show that global mean surface air temperature of the cpl_4×CO_2 run is a linear combination of the temperature increases of the amip_4×CO_2 and amip_4K runs, i.e.,

$$\Delta\overline{T}^{4x} = \Delta\overline{T}^{4xP0} + \Delta\overline{T}^{P4}$$

where $\Delta\overline{T}^{4x}$ is the global mean surface air temperature increase in the cpl_4×CO_2, $\Delta\overline{T}^{4xP0}$ is the global mean surface air temperature increase due to CO_2 quadrupling with fixed SST (amip_4×CO2), and $\Delta\overline{T}^{P4}$ is the global mean surface air temperature increase due to 4K SST uniform increase without CO_2 change (amip_4K).

2.2 Response of WNPSH to global warming

The response of the mean state of the EASM to the global warming scenario is evaluated by comparing the climatological May-June-July-August (MJJA) mean precipitation and

Table 1 Summary of model simulations

Model type	Name	SST	CO_2 (ppmv)	Initial conditions	Simulation years
Coupled	pdControl	Calculated by model	1x	CCSM4 twentieth century	2006–2155, 150 years
	cpl_4×CO_2	Calculated by model	4x	Same as above	2006–2155, 150 years
Atmosphere only	amip_4×CO_2	Observation, 1949–2001 average climatology	4x	Same as above	2006–2040, 35 years
	amip_4K	Observation + 4K	1x	Same as above	2006–2040, 35 years
	amip_sst	SST from cpl_4×CO_2	1x	cpl_4×CO_2 restart	2121–2154, 34 years
	amip_lhflx*	SST from cpl_4×CO_2	1x	cpl_4×CO_2 restart	2121–2154, 34 years

*Latent heat flux of cpl_4×CO_2 was restored over the tropical western Pacific region (105–140° E, 5° S–12.5° N)

geopotential height (GPH) in pdControl, cpl_4×CO_2, amip_4×CO_2, and amip_4K (Fig. 1). Due to the close relationship between EASM precipitation and the WNPSH, we first explore the mechanisms responsible for the WNPSH changes in the global warming scenario. The most prominent difference in precipitation between pdControl run and cpl_4×CO_2 is the equatorward displacement of the Intertropical Convergence Zone (ITCZ) in the cpl_4×CO_2 run (Fig. 1a–c). The mean rainfall over SCS and the tropical Pacific Ocean is noticeably reduced in the cpl_4×CO_2 run compared to the pdControl run, and intensifies over the EASM region to the north of 20° N (Fig. 1c) in the cpl_4×CO_2 run. These changes in precipitation are associated with changes in the position and amplitude of the WNPSH. In the pdControl run, the western edge of the 1540 m isopleth reaches 160° E; the ridge line of the WNPSH is located along 30° N and tilts northward when it approaches the East Asian continent (Fig. 1a). In the cpl_4×CO_2 run, the WNPSH intensifies and extends westward: the isopleth of 1540 m reaches 140° E and the western portion of the WNPSH tilts southward (Fig. 1b). These results are consistent with findings of previous studies (e.g., Hu et al. 2003; Kimoto 2005; Kripalani et al. 2007; Lee and Wang 2014).

Both amip_4×CO_2 and amip_4K runs exhibit enhanced precipitation extending from SCS to WP. This excessive precipitation can be related to the lack of air-sea interaction in the AMIP-type simulations. In amip_4×CO_2 (Fig. 1d), which shows the response of the EASM to rapid atmospheric warming, the WNPSH is displaced eastward compared with its location in the cpl_4×CO_2 (Fig. 1b) simulation. In amip_4×CO_2 (Fig. 1d), the western edge of the 1540 m isopleth is located around 160° E, which is 20° eastward compared to cpl_4×CO_2 (Fig. 1b). This implies that the enhanced precipitation over SCS and nearby WP due to the lack of air-sea interaction prevents the WNPSH from extending westward. The amip_4K (Fig. 1e) shows the EASM response to the SST warming, and the precipitation over SCS and nearby WP in this simulation is more intense than that in the amip_4×CO_2 (Fig. 1f). However, the WNPSH does not retreat eastward as expected. The western edge of the 1540 m isopleth extends to around 150° E, which is displaced 10° westward compared to amip_4×CO_2 (Fig. 1d, e). This indicates that the atmospheric response due to warming of boundary conditions plays a more important role in changing the EASM mean state than the atmospheric warming in response to the CO_2 forcing.

Therefore, the results of this analysis suggest that changes in the WNPSH under the global warming scenario can be affected by two factors: (1) the warming of the boundary conditions that favors the amplification of the WNPSH and (2) the convective activity driven by the

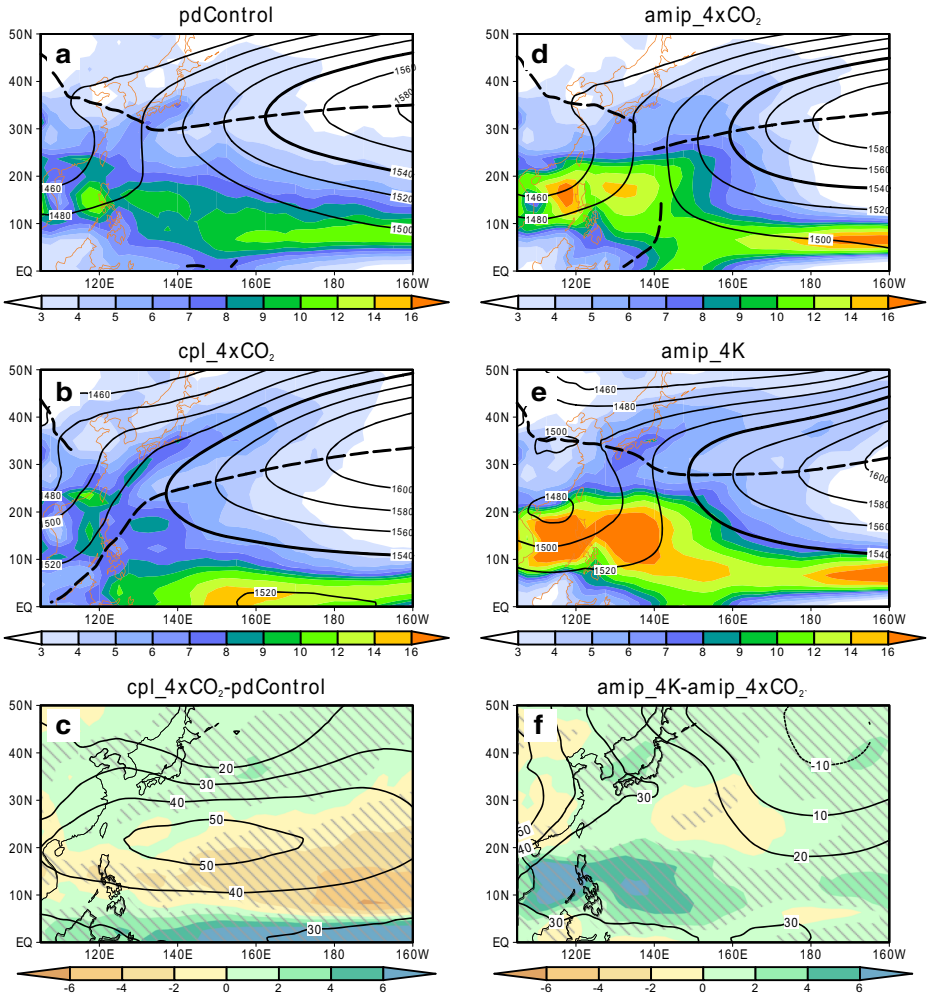

Fig. 1 MJJA mean precipitation rate (shadings, unit: mm/day) and GPH at 850-hPa (contours, unit: m). **a** pdControl. **b** cpl_4×CO_2. **c** Difference between cpl_4×CO_2 and pdControl. **d** amip_4×CO_2. **e** amip_4K. **f** Difference between amip_4K and amip_4×CO_2. The bold black contour in **a**, **b**, **d**, and **e** denotes the 1540 m isopleth, and the dashed black line in these four panels denotes subtropical ridge. The gray slashes in **c** and **f** denote the region where the precipitation difference is above the 95% significance level. The difference of 850-hPa GPH is plotted only in the regions where it exceeds the 95% significance level

underlying air-sea interactions over tropical SCS and nearby WP that controls the location of the WNPSH.

3 The air-sea interaction mechanism

3.1 Model simulations

The proposed mechanisms explaining the changes in the WNPSH under warmer climate conditions can be tested in an intervention experiment designed to alter the air-sea interaction

only over the region of interest. Because the mean SST used to construct the boundary conditions of the amip_4K experiment is not consistent with the mean state of the coupled run, the intervention experiment was done in two steps: (i) A control-type experiment, hereafter amip_sst, in which the SSTs from the last 34 years (2121–2154) of cpl_4×CO_2 simulation are used as boundary conditions, while the atmospheric CO_2 concentration is the same as in the pdControl simulation. In this experiment, the atmospheric variability is influenced by the prescribed variability of SST simulated by cpl_4×CO_2. If the atmospheric CO_2 in amip_sst is quadrupled, then the atmospheric response of this run should be the same as in cpl_4×CO_2. (ii) A sensitivity-type experiment, hereafter amip_lhflx, which uses the same configuration as the amip_sst run, except over a small region over SCS and WP where the surface evaporation is altered to restore the surface latent heat flux (LHFLX) at the levels of the cpl_4×CO_2 simulation (see details below). The underlying assumption of this experiment is that increased surface evaporation enhances the probability of convective precipitation (Cui and Li 2006). The expectation is that this reduction of convective activity over SCS and WP relative to the amip_sst run will impact EASM precipitation via changes in the WNPSH position. The specifics of these two experiments are summarized in Table 1.

The region in the tropical WP with the largest influence on EASM precipitation is determined as follows: (a) define a precipitation index as the average over the area (115–140° E, 12.5–20° N) where the square of the difference of MJJA precipitation between cpl_4×CO_2 and amip_sst has a maximum (Fig. 2a). This index measures the daily precipitation variance between the two simulations; (b) calculate the correlation between the precipitation index defined in (a) and the LHFLX difference between cpl_4×CO_2 and amip_sst (Fig. 2c). The maximum correlation is over the tropical WP, which means that changes of precipitation over the subtropics are strongly related to the changes of LHFLX over the tropics. To verify whether the tropical convection affects the WNPSH, a similar calculation was done for LHFLX and GPH. The LHFLX index is calculated as the area average over (105–140° E, 5° S–12.5° N), where the LHFLX difference between cpl_4×CO_2 and amip_sst is the largest (Fig. 2b). This area also contains the largest correlation obtained in step (b). The correlation between the LHFLX index and GPH difference between cpl_4×CO_2 and amip_sst (Fig. 2d) indicates that strong (weak) convective activity over tropical WP is related to the eastward (westward) displacement of the WNPSH. The distribution of the MJJA mean LHFLX difference between cpl_4×CO_2 and amip_sst shows that over tropical WP, the LHFLX in cpl_4×CO_2 is around 10 W/m^2 less than in amip_sst (Fig. 2b).

The LHFLX deficiency over tropical WP in cpl_4×CO_2 is mimicked in the amip_lhflx experiment. In the amip_lhflx experiment, the LHFLX is subtracted from the amip_sst experiment at each time step and at each grid point in the tropical WP domain (105–140° E, 5° S–12.5° N). Figure 3 shows the area average (105–140° E, 5° S–12.5° N) of the MJJA mean LHFLX difference between cpl_4×CO_2 and amip_sst from year 2121 to 2154 (blue line). The average of the LHFLX difference is ~− 10 W/m^2. As mentioned above, this difference of − 10 W/m^2 is added to the amip_lhflx experiment at each grid point during MJJA in each year. The area average of LHFLX difference between amip_sst and amip_lhflx (red line) shows that the mean difference of LHFLX between these two experiments is ~− 12 W/m^2.

3.2 The sensitivity of WNPSH to SST warming

The climatological MJJA mean precipitation of the EASM was compared among pdControl, amip_sst, and cpl_4×CO_2 (Fig. 4). The comparison of amip_sst to pdControl (Fig. 4d) gives an

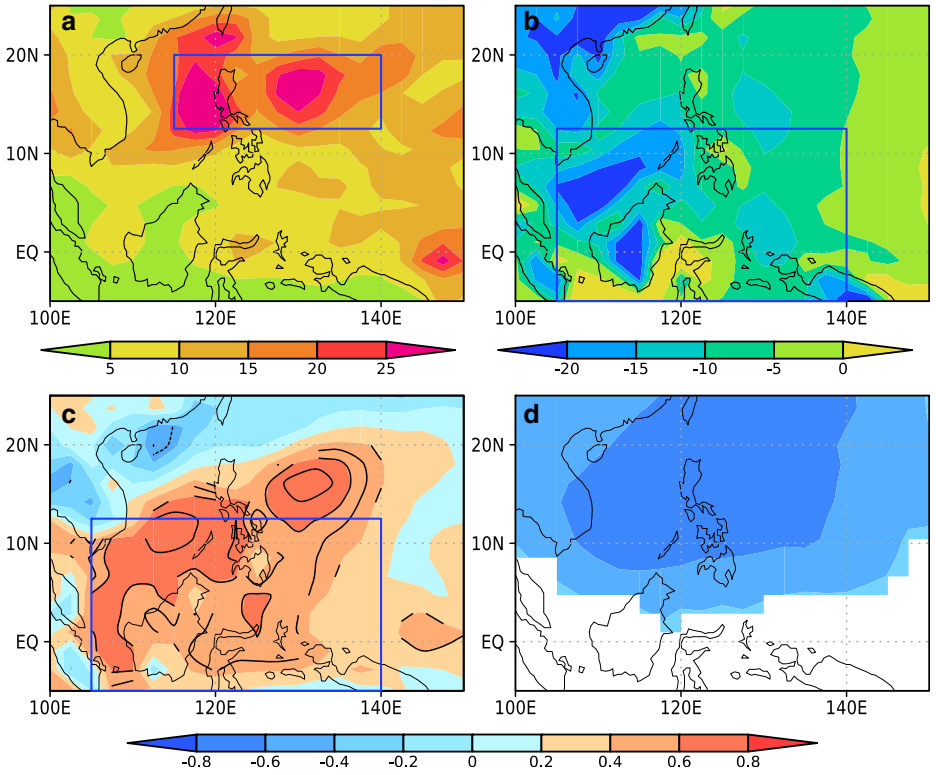

Fig. 2 **a** Variance of the MJJA mean precipitation: cpl_4×CO_2 minus amip_sst (unit: mm^2/day^2). **b** MJJA mean LHFLX: cpl_4×CO_2 minus amip_sst (unit: W/m^{-2}). **c** Correlation coefficient between the precipitation difference index (area averaged precipitation difference over the blue box in (**a**)) and the LHFLX difference between cpl_4×CO_2 and amip_sst. Black contours enclose the region where the correlation coefficient exceeds the 95% significance level. **d** Correlation coefficient between LHFLX difference index (area averaged LHFLX difference over the blue box in **c**) and 850-hPa GPH difference between cpl_4×CO_2 and amip_sst. Only the area which exceeds the 95% significance level is shaded

estimation of the EASM response to SST warming, whereas the comparison of amip_sst to cpl_4×CO_2 (Fig. 4e) is intended to estimate the effects of the air-sea feedbacks. The response of EASM precipitation to the surface warming in the amip_sst experiment shows a large amount of precipitation over SCS and adjacent WP, southern China, and south of Japan (Fig. 4b). Because this increase of precipitation is consistent with the results seen for the amip_4×CO_2 and amip_4K simulations (Fig. 1d, e), we can now eliminate the possibility that changes noticed in the AMIP-type simulations with prescribed observed SST were different from the changes in the cpl_4×CO_2 run due to differences between the coupled model SST and observed SST. The difference between the amip_sst and cpl_4×CO_2 runs (Fig.4e) suggests that the lack of coupling induces stronger precipitation over SCS, WP, and the region to the north of 30° N in response to the global warming.

Because EASM precipitation is affected by the position of the WNPSH and its associated moisture transport, their response to global warming in the uncoupled simulation is also compared to the coupled response (Fig. 5). In the amip_sst experiment, the western edge of the WNPSH is located around 5° to the east of the WNPSH in cpl_4×CO_2. This indicates that the warming of the boundary conditions favors the intensification and westward extension of

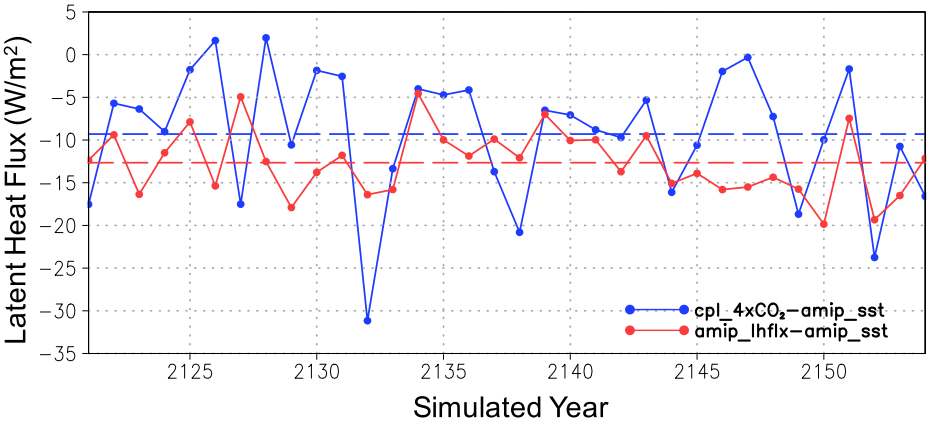

Fig. 3 Difference of MJJA mean area averaged LHFLX (105°–140° E, 5° S–12.5° N) (dotted lines) and the mean of the difference (dashed lines). Blue lines correspond to cpl_4×CO_2 minus amip_sst. Red lines correspond to amip_lhflx minus amip_sst

the WNPSH. However, the lack of the air-sea feedback in the amip_sst experiment inhibits the WNPSH from extending as far westward as in cpl_4×CO_2.

The westward extension of the WNPSH changes the low-level circulation and the moisture transport. In the pdControl run, the moisture from SCS flows northward into East Asia, merging with the northward moisture transport from WNP (Fig. 6a). In the amip_sst experiment, the enhanced moisture is transported by southwesterly flow over East Asia (Fig. 6b). This northeastward moving moisture transport is further amplified in cpl_4×CO_2, where a band of intense moisture develops from northern SCS to northern Japan (Fig. 6c). In addition, compared with cpl_4×CO_2, the moisture transport in amip_sst is reduced over the subtropical monsoon trough (from South China to southern Japan) and is increased over eastern SCS and adjacent WP. The difference in the moisture transport between amip_sst and cpl_4×CO_2 is related to the shape of the WNPSH. For instance, the 1520 m isopleth in amip_sst is almost parallel to the 130° E longitude (Fig. 6b), whereas in cpl_4×CO_2, the 1520 m isopleth tilts northeastward and is located closer to East Asia (Fig. 6c). Therefore, in the amip_sst simulation, the moisture transport from South China to southern Japan is weaker than in cpl_4×CO_2. The difference in moisture transport is consistent with the difference in precipitation between amip_sst and cpl_4×CO_2 (Fig. 4e).

3.3 The comparisons between amip_sst and amip_lhflx

In this section, the EASM simulated by amip_sst and amip_lhflx experiments will be analyzed, including the seasonal mean state and annual cycle. Because the amip_lhflx simulation was constructed to mimic the mean conditions over the tropical WP of the cpl_4×CO_2 simulation, the results of cpl_4×CO_2 are also included in the analysis.

3.3.1 The relationship between EASM precipitation and the WNPSH

The impact of reducing the surface evaporation over the tropical WP on the position of the WNPSH is shown in Fig. 7, which shows the MJJA mean values of the westernmost and easternmost contours of the 1540 m isopleth of GPH. The position of WNPSH varies between

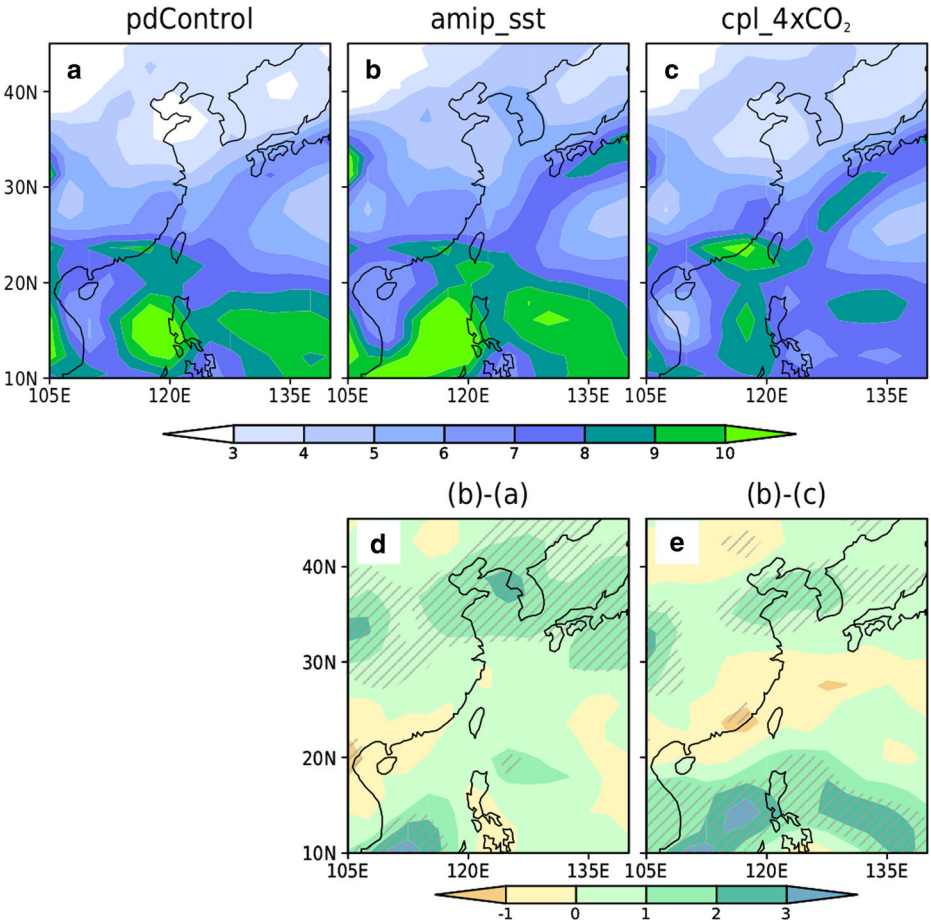

Fig. 4 **a**–**c** MJJA mean precipitation rate for pdControl, amip_sst, and cpl_4×CO_2, respectively (unit: mm/day). **d** amip_sst minus pdControl. **e** amip_sst minus cpl_4×CO_2. The gray slashes in **d** and **e** denote the region where the difference of precipitation exceeds the 95% significance level

120°–150° E in cpl_4×CO_2, 128°–155° E in amip_sst, and 120°–152° E in amip_lhflx. By making the convective activity over the tropical WP similar to the coupled simulation, the WNPSH simulated by amip_lhflx responds by changing its position, which varies within the same range as in the coupled simulation. This result implies that the position of the WNPSH during the boreal summer is sensitive to the air-sea interactions over SCS and tropical WP.

To further evaluate the link between the WNPSH and EASM precipitation, canonical correlation analysis (CCA, Supplemental) was applied to 850-hPa GPH and precipitation. The analysis was performed on each of the three simulations: cpl_4×CO_2, amip_sst, and amip_lhflx (Fig. 8). In cpl_4×CO_2 and amip_lhflx, two PCs of precipitation and three PCs of GPH are retained. In amip_sst, the data is truncated to two PCs of precipitation and four PCs of GPH.

The variance explained by the first CCA pair is comparable in the three experiments, with the exception that the variance explained by precipitation is higher in amip_lhflx (Fig. 8e) compared to the other two simulations. The first CCA pattern of precipitation reveals a dipole

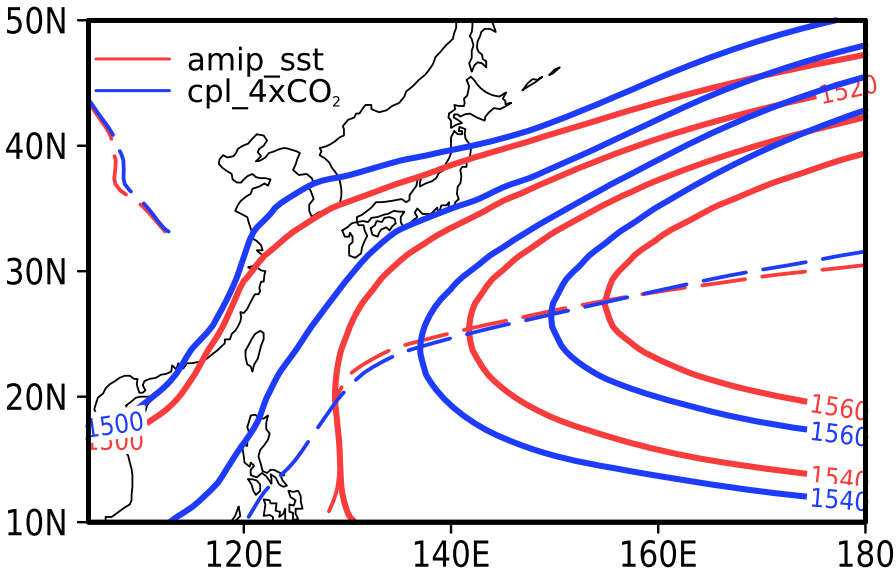

Fig. 5 MJJA mean GPH at 850-hPa in amip_sst (red) and cpl_4×CO_2 (blue). Dashed line denotes the subtropical ridge

structure in the meridional direction in all the three simulations: negative anomalies over SCS and tropical WP, and positive anomalies to its north (Fig. 8a, c, e). The position and magnitude of the GPH anomaly show some variations among the three experiments. In amip_sst (Fig. 8b), the region of maximum GPH anomaly is smaller and tilts northeastward compared to the GPH pattern of the other two simulations. In the amip_lhflx run (Fig. 8f), the region of maximum GPH anomaly covers the same area as in cpl_4×CO_2 (Fig. 8d), and the position at around 20° N is consistent with the coupled run.

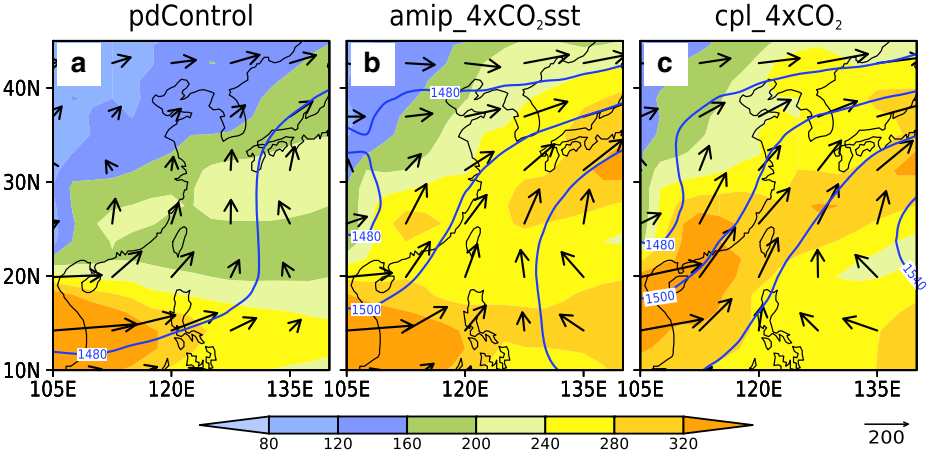

Fig. 6 MJJA climatology of 850-hPa GPH (contours), vertically integrated moisture flux direction (vectors), and magnitude (shadings). **a** pdControl. **b** amip_sst. **c** cpl_4×CO_2. Units: m for GPH; kg/m/s for moisture flux. The isopleths for 850-hPa GPH are 1480 m, 1500 m, 1520 m, and 1540 m

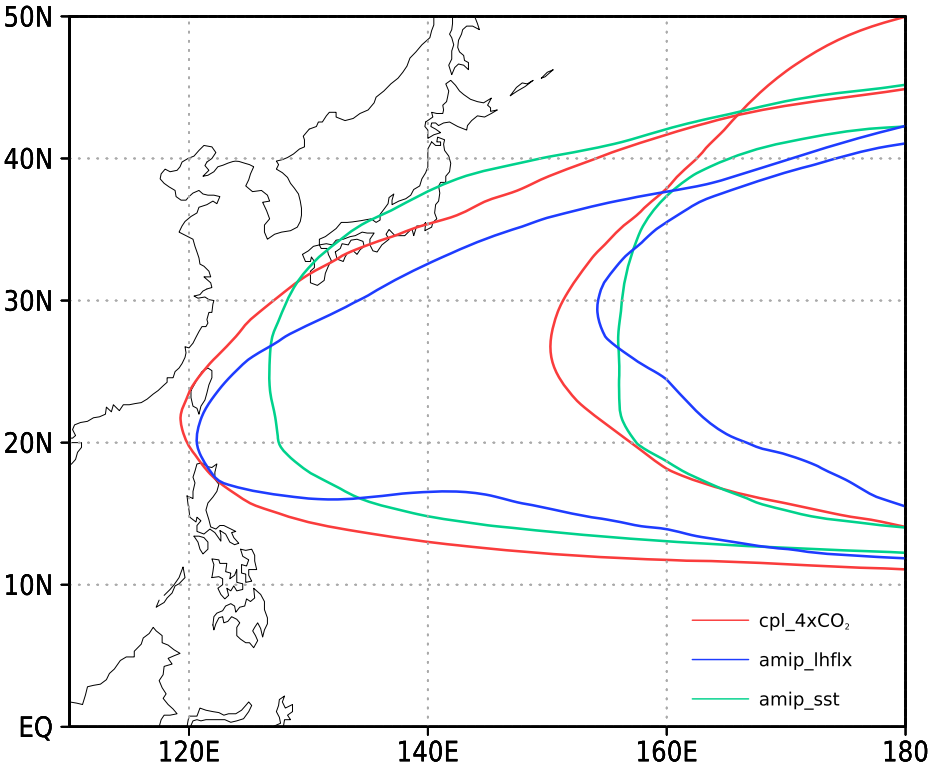

Fig. 7 The MJJA mean of the envelope of WNPSH positions described as the westernmost and easternmost contour of 1540 m isopleth of 850-hPa GPH

One feature not captured by the two AMIP-type simulations is the negative GPH anomaly over the mid-latitudes of the coupled simulation (Fig. 8d), suggesting that the relationship between EASM precipitation and the large-scale circulation of mid-latitudes is independent of the convective activity over SCS and tropical WP.

The CCA analysis shows that weak convection over SCS and tropical WP yields to the westward displacement of the WNPSH, which further influences EASM precipitation by changing the southwesterlies and moisture transport to the EASM domain. It also shows that changes of LHFLX in amip_lhflx, although small, reproduce the features of the cpl_4×CO_2 simulations. This result suggests that the response of EASM precipitation to global warming depends on the response of air-sea interactions in SCS and tropical WP to the increase in the external forcing. The connection between the tropics and EASM precipitation is established through the WNPSH, which channels the tropical flow and moisture transport into the subtropics.

3.3.2 Seasonal cycle of the EASM

The seasonal cycle of precipitation is another element of the EASM system affected by climate change. To evaluate the seasonal cycle of the relationship between EASM precipitation and the WNPSH, a GPH index that represents the position of the WNPSH is calculated following the method of Zhang and Tao (1999). The GPH index indicates the mean latitude of the western

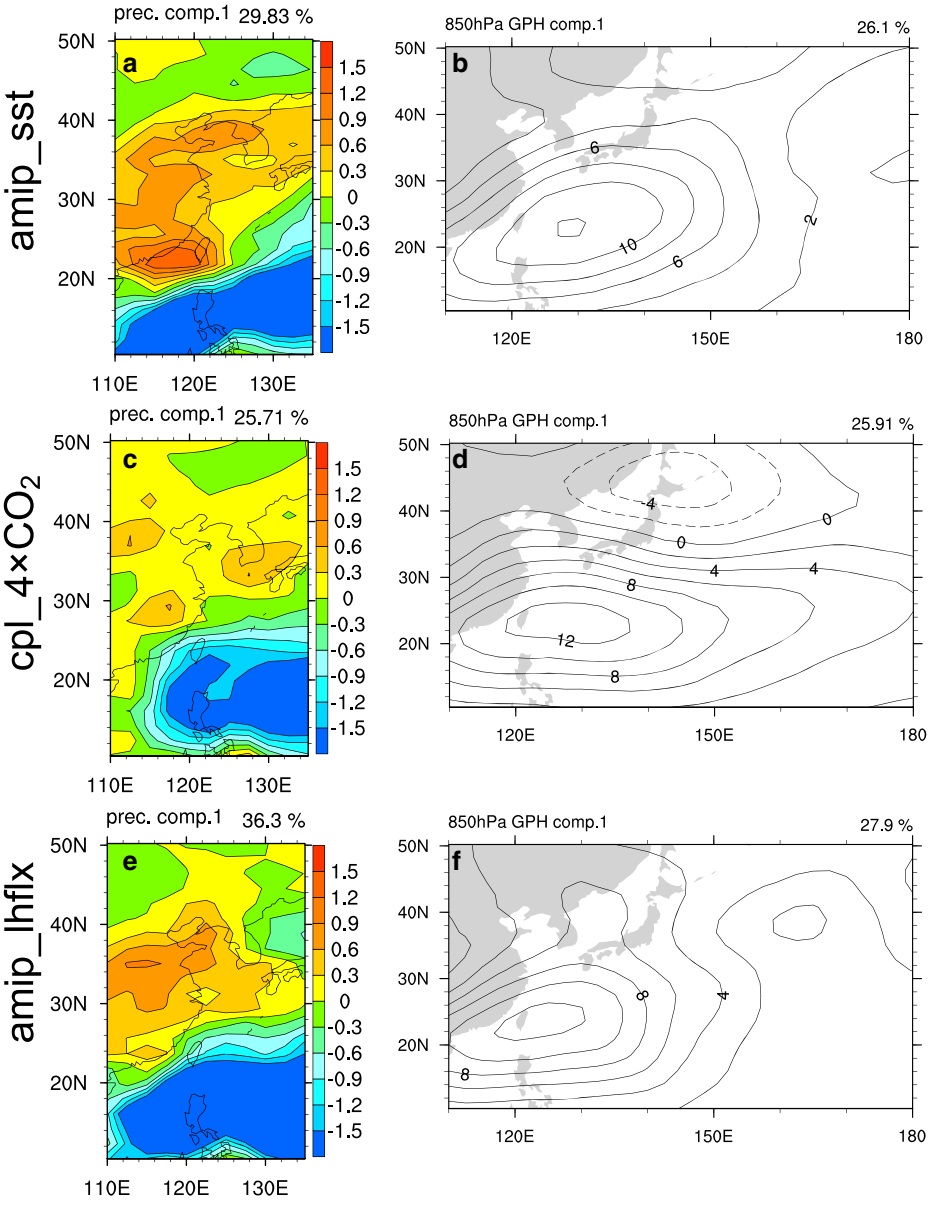

Fig. 8 First pattern of CCA of precipitation (shadings, left column) and 850-hPa GPH (contours, right column). **a**, **b** amip_sst. **c**, **d** cpl_4×CO_2. **e**, **f** amip_lhflx

edge of the WNPSH and is calculated as the latitude where the 850-hPa zonal wind between 115° and 140° E is zero. The impact of tropical WP air-sea interactions on the response of the seasonal cycle of precipitation can be evaluated by comparing the cpl_4×CO_2 run and AMIP-type experiments (Fig. 9).

The seasonal cycle of GPH index shows consistency with the precipitation in amip_sst, cpl_4×CO_2, and amip_lhflx simulations (Fig. 9a–c). In amip_sst (Fig. 9a), the onset of the

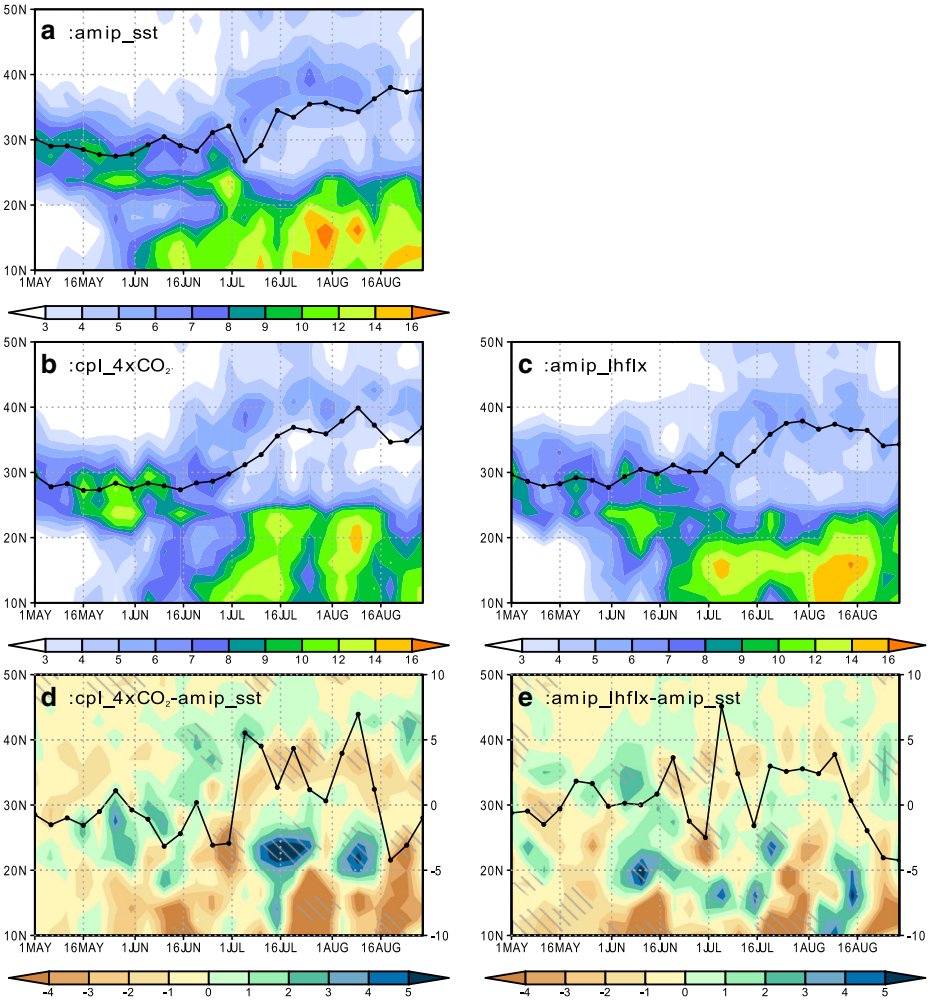

Fig. 9 Annual cycle of precipitation (shadings) averaged between 110° and 120° E and 850-hPa GPH index (black line) based on pentads. **a** amip_sst. **b** cpl_4×CO_2. **c** amip_lhflx. **d** cpl_4×CO_2 minus amip_sst. **e** amip_lhflx minus amip_sst. The gray slashes in **d** and **e** denote the regions where the precipitation difference exceeds the 95% significance level. The *y*-axis on the right side in **d** and **e** denotes the difference of the WNPSH index. Precipitation and precipitation difference unit: mm/day

EASM occurs around the 16th of May, when the tropical rain band merges with the rain band north of 20° N. Around the 16th of June, the monsoonal rain belt moves northward and stays between 30° N and 34° N, indicating the onset of the Mei-yu season, which represents a ramification of the EASM in subtropical East Asia (Ding and Chan 2005). The Mei-yu rainfall lasts until the beginning of July when the monsoonal rain belt jumps northward again and reaches 40° N. The precipitation persists between 35° and 40° N during mid-July and the beginning of August and starts retreating southward in early August. The timing of the three jumps of the rain belt in the amip_sst simulation are similar to those in cpl_4×CO_2 (Fig. 9b). However, in cpl_4×CO_2, there is more precipitation during the first standing stage between 20° and 30° N, the rain band reaches north of 40° N during July and August, and there is less

rainfall between 30° and 40° N (Fig. 9b, d). In amip_lhflx (Fig. 9c), the onset of the EASM occurs 10 days later than in amip_sst (Fig. 9a), and this is about the same time as the onset of the EASM in cpl_4×CO_2 (Fig. 9b). The Mei-yu precipitation in amip_lhflx is larger than in the amip_sst simulation, although smaller than in cpl_4×CO_2. This suggests that the onset of the Mei-yu season is strongly modulated by the convective activity in the equatorial WP, whereas the amount of rainfall is only partially explained by the mean state of the equatorial WP. In early July, the rain band in amip_lhflx jumps northward and stays between 35° and 40° N until mid-August. The difference plot between amip_sst and amip_lhflx (Fig. 9e) does not show large differences towards the end of the season. This result suggests that towards the end of the monsoon season, the tropical influence on the EASM is weaker than in the beginning of the season. The amip_lhflx experiment is designed to simulate an EASM with similar characteristics as in cpl_4×CO_2. The expectation is that differences between amip_sst and cpl_4×CO_2 are similar to differences between amip_sst and amip_lhflx. The inspection of Fig. 9d, e shows that in both cases, the difference in precipitation follows the same meridional migration as the WNPSH difference, and a lack of precipitation over 10°–20° N persists in both figures, especially during May and June. This indicates that the seasonal cycle of the WNPSH is also sensitive to the air-sea interactions over the tropical WP.

The influence of LHFLX changes in the tropics on the seasonal cycle of EASM precipitation through the WNPSH is presented in Fig. 10, which shows the monthly mean evolution of the low-level wind and GPH for amip_sst and its difference from cpl_4×CO_2 and amip_lhflx. In amip_sst, during May and June, a southwesterly flow prevails over East Asia, which resides at the northwestern edge of the WNPSH. This southwesterly flow changes its direction and magnitude with the changes in the WNPSH, i.e., in July and August when the WNPSH moves northward, southwesterlies over East Asia turn into southeasterlies (Fig. 10a). In cpl_4×CO_2 (Fig. 10b), the WNPSH is stronger than in amip_sst in almost every month. Only in May, the northern branch of the WNPSH, which is located poleward of 20° N, in amip_sst is stronger than in the coupled simulation, and the difference is significant over East China. In July and August, the anomalies of wind and GPH show a large-scale wave pattern. In amip_lhflx (Fig. 10c), the WNPSH intensifies compared to amip_sst, except in July when it is weaker. Compared with Fig. 10b, the magnitude of the WNPSH in amip_lhflx is smaller than in cpl_4×CO_2 and changes in the WNPSH do not exceed the 95% significance level in July and August. From May to August, the reduced convection over SCS and WP induces an anticyclonic anomaly over northern SCS. However, the magnitude and location of this anomaly vary. In May, positive GPH anomalies dominate over SCS and southern Japan, along with anticyclonic anomalies there. In June, two centers of positive GPH anomaly develop over SCS and to the east of Japan. The westerlies (southwesterlies) on the northern (northwestern) flank of the GPH anomalies strengthen the southwesterly flow from northern SCS to southern Japan. In July, the anticyclonic anomaly over SCS is displaced westward and two centers of negative GPH anomaly form over subtropical WP, along with cyclonic anomalies there. In August, anticyclonic anomalies dominate over SCS and southern China. However, the northerly anomalies on the eastern side of the anticyclonic anomaly reduce the prevailing southerly flow.

The results in Fig. 10 suggest that the air-sea interaction in the equatorial western Pacific affects the intensity of circulation and position of the equatorial branch of the WNPSH. A decrease of LHFLX over the tropics leads to a Gill-type off-equatorial response to the north of the heating anomaly and results in a Rossby wave train propagating northeastward from the tropical regions into the mid-latitude Pacific Ocean. This wave train can be attributed to the

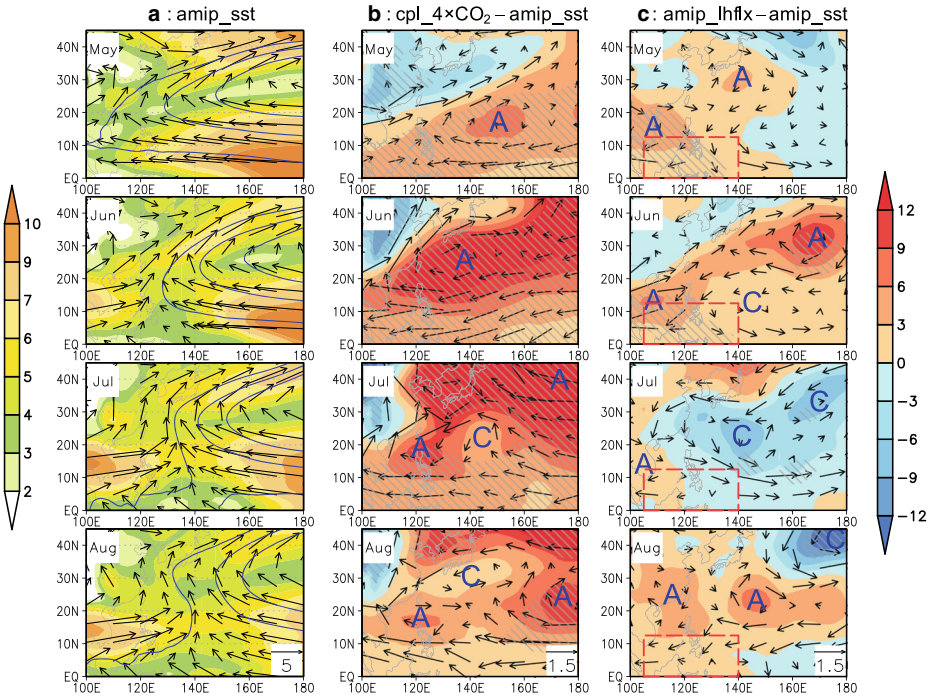

Fig. 10 Wind and GPH at 850 hPa from May to August for **a** amip_sst, **b** cpl_4×CO_2 minus amip_sst, and **c** amip_lhflx minus amip_sst. In column **a** shadings denote magnitude of the wind, vectors show the directions of horizontal wind, and contours are the isopleths of 1520, 1540, and 1560 m. In columns **b** and **c** shadings denotes the difference of 850-hPa GPH (unit: m), and vectors denote the difference of wind. Gray slashes denote the regions where the GPH difference is above 95% significance level. "A" denotes anticyclonic anomaly, and "C" denotes cyclonic anomaly. The red box in **c** column denotes the area where the LHFLX is reduced in the amip_sst experiment

diabatic heating anomalies related to EASM precipitation (Zhang et al. 2016) and it can feedback onto the WNPSH variability (Seo et al. 2012). The southwesterly anomaly within the anticyclonic circulation intensifies the southwesterly flow on the northwestern edge of the WNPSH, thus strengthening the WNPSH, and the western edge of the high moves westward. The westward displacement of the WNPSH allows the tropical westerlies to advance into the western Pacific before being deflected northward and the supply of moisture flux into the EASM domain is enhanced. The lack of response in amip_lhflx during July and August suggests that during these months, the EASM is dominated by extratropical influences, and the tropical forcing may be of secondary importance.

4 Summary and discussions

The response of the EASM to global warming was investigated in ocean-atmosphere coupled and uncoupled simulations with a GCM using super-parameterization of cloud processes. In the coupled simulation, the seasonal mean precipitation increases by 20–30% as a result of global warming. The uncoupled simulations also project a positive trend of EASM precipitation, and the increase is slightly higher than in the simulation with fully interactive air-sea

interactions. The EASM response to global warming tends to be dominated by changes in surface conditions and is sensitive to the remote influence of changes in the air-sea interactions in the deep tropics (15° S–15° N).

The effect of air-sea interaction in the tropics is felt in the EASM region through changes in the position and intensity of the WNPSH. The WNPSH can also be affected by global warming (Li et al. 2010; Xiang et al. 2013). The effects of tropical air-sea interactions on the WNPSH were separated from the global warming response in a sensitivity-type experiment in which the surface latent heat was changed only over a small domain over SCS and the adjacent WP.

The decrease of LHFLX over SCS and adjacent WP yields a Rossby wave response (anticyclonic circulation) to the north of the forcing, extending over East Asia. The Rossby wave response is associated with winds that enhance the mean monsoonal flow and position of the WNPSH. Other studies also suggest that the enhancement of the EASM is through a Gill-type response (e.g., Li et al. 2010); however, in these studies, the source of heating is attributed to the basin-scale warming of the IO. Our results suggest that air-sea fluxes in the SCS and adjacent WP affect EASM precipitation through the large-scale circulation of the subtropics associated with the WNPSH. The domain of influence on the WNPSH, and subsequently the EASM, revealed by this study appears to be different from the regions where the local wind-evaporation feedbacks and ENSO forcing have been found by Xiang et al. (2013) to exert an influence on the summer variability of the WNPSH during present day climate conditions.

In the amip_sst and amip_lhflx simulations, the IO air-sea interactions and the land-sea temperature contrasts are consistent with their counterparts in the coupled run. Therefore, the resulting changes can be interpreted as being due to air-sea interactions over the tropical western Pacific.

In the framework revealed by this study, the global warming induced by the atmospheric CO_2 forcing reduces the surface evaporation and convective heating over SCS and the adjacent WP. This negative heating anomaly affects the large-scale circulation associated with the WNPSH, which further impacts EASM precipitation.

Another interesting result of this study is the finding that the slow and fast response of EASM precipitation to the CO_2 atmospheric forcing have the same pattern, unlike the conventional parameterized models that appear to show opposite patterns (Chen and Bordoni 2016). Cumulus parameterization details can substantially affect EASM precipitation (Choi et al. 2015) and model climate sensitivity (Zhao 2014).

This type of study could be applied to other regions identified as having an influence on the EASM such as the North Atlantic Ocean (e.g., Yu et al. 2009; Wang et al. 2009), other modes of atmospheric variability such as the Artic Oscillation (Gong and Ho 2003; Gong et al. 2011), and changes in snow cover/snow depth (Pu and Xu 2009).

Acknowledgements CS is grateful to Drs. Mariana Vertenstein and Phil Rash for their invaluable assistance during the design of the sensitivity-type experiment.

Funding information The work was supported by the National Science Foundation and Technology Center for Multi-scale Modeling of Atmospheric Processes managed by Colorado State University under cooperative agreement no. ATM-0425247.

References

Bretherton CS, Blossey PN, Stan C (2014) Cloud feedbacks on greenhouse warming in the superparameterized climate model SP-CCSM4. J Adv Model Earth Syst 6:1185–1204. https://doi.org/10.1002/2014MS000355

Cevuturi A, Klingaman NP, Turner AG, Hannah S (2018) Projected changes in the Asian-Australian monsoon region in 1.5°C and 2°C global-warming scenarios. Earth's Future 6:339–358. https://doi.org/10.1002/2017EF000734

Chen J, Bordoni S (2016) Early summer response of the East Asian summer monsoon to atmospheric CO2 forcing and subsequent sea surface warming. J Clim 29:5431–5446. https://doi.org/10.1175/jcli-d-15-0649.1

Choi I-J, Jin EK, Han J-Y, Kim S-Y, Kwon Y (2015) Sensitivity of diurnal variation in simulated precipitation during East Asian summer monsoon to cumulus parameterization schemes. J Geophys Res Atmos 120:11, 971–911,987. https://doi.org/10.1002/2015JD023810

Cui X, Li X (2006) Role of surface evaporation in surface rainfall processes. J Geophys Res Atmos 111:n/a–n/a. https://doi.org/10.1029/2005JD006876

Ding Y, Chan JCL (2005) The East Asian summer monsoon: an overview. Meteor Atmos Phys 89:117–142. https://doi.org/10.1007/s00703-005-0125-z

Ding Y, Wang H, Wang B (2005) East Asian monsoon: East Asia, paper presented at International Committee of the Third International Workshop on Monsoons (IWM-III), Hangzhou, China

Gill AE (1980) Some simple solutions for heat-induced tropical circulation. Quart J Roy Meteor Soc 106:447–462. https://doi.org/10.1002/qj.49710644905

Gong DY, Ho CH (2003) Artic oscillation signals in East Asian summer monsoon. J Geophys Res 108:4066. https://doi.org/10.1029/202JD002193

Gong DY, Yang J, Kim SJ, Gao Y, Guo D, Zhou T, Hu M (2011) Spring artic oscillation-East Asian summer monsoon connection through circulation changes over the western North Pacific. Clim Dyn 37:2199–2216. https://doi.org/10.1007/s00382-0111041-1

He J, Ju J, Wen Z, Lü J, Jin Q (2007) A review of recent advances in research on Asian monsoon in China. Adv Atmos Sci 24:972–992. https://doi.org/10.1007/s00376-007-0972-2

He B, Yang S, Li Z (2016) Role of atmospheric heating over the South China Sea and western Pacific regions in modulating Asian summer climate under the global warming background. Clim Dyn 46:2897–2908. https://doi.org/10.1007/s00382-015-2739-2

Hensen J et al (2005) Efficacy of climate forcings. J Geophys Res 110:D18104

Hu Z-Z, Yang S, Wu R (2003) Long-term climate variations in China and global warming signals. J Geophys Res 108:n/a–n/a. https://doi.org/10.1029/2003JD003651

Huang R, Sun F (1992) Impacts of the tropical Western Pacific on the East Asian summer monsoon. J Meteorol Soc Japan Ser II 70:243–256. https://doi.org/10.2151/jmsj1965.70.1B_243

Huang G, Hu K, Xie S-P (2010) Strengthening of tropical Indian Ocean teleconnection to the Northwest Pacific since the mid-1970s: an atmospheric GCM study. J Clim 23:5294–5304. https://doi.org/10.1175/2010jcli3577.1

Hurrell JW, Hack JJ, Shea D, Caron JM, Rosinski J (2008) A new sea surface temperature and sea ice boundary dataset for the community atmosphere model. J Clim 21:5145–5153. https://doi.org/10.1175/2008jcli2292.1

Kimoto M (2005) Simulated change of the East Asian circulation under global warming scenario. Geophys Res Lett 32:n/a–n/a. https://doi.org/10.1029/2005GL023383

Kitoh A, Uchiyama T (2006) Changes in onset and withdrawal of the East Asian summer rainy season by multi-model global warming experiments. J Meteorol Soc Jpn Ser II 84:247–258. https://doi.org/10.2151/jmsj.84.247

Kripalani RH, Oh JH, Chaudhari HS (2007) Response of the East Asian summer monsoon to doubled atmospheric CO2: coupled climate model simulations and projections under IPCC AR4. Theor Appl Climatol 87:1–28. https://doi.org/10.1007/s00704-006-0238-4

Kurihara K et al (2005) Projection of climatic change over Japan due to global warming by high-resolution regional climate model in MRI. Sci Online Lett Atmos 1:97–100. https://doi.org/10.2151/sola.2005-026

Kusunoki S, Arakawa O (2012) Change in the precipitation intensity of the East Asian summer monsoon projected by CMIP3 models. Clim Dyn 38: 2055–2072. https://doi.org/10.1007/s00382-011-1234-7

Lee J-Y, Wang B (2014) Future change of global monsoon in the CMIP5. Clim Dyn 42:101–119. https://doi.org/10.1007/s00382-012-1564-0

Li J, Wu Z, Jiang Z, He J (2010) Can global warming strengthen the East Asian summer monsoon? J Clim 23:6696–6705. https://doi.org/10.1175/2010jcli3434.1

Li W, Li L, Ting M, Liu Y (2012) Intensification of Northern Hemisphere subtropical highs in a warming climate. Nat Geosci 5:830–834
Li Z, Yang S, He B, Hu C (2016) Intensified springtime deep convection over the South China Sea and the Philippine Sea dries southern China. Sci Rep 6:30470
Lu R (2001) Interannual variability of the summertime North Pacific subtropical high and its relation to atmospheric convection over the warm pool. J Meteor Soc Japan Ser II 79:771–783. https://doi.org/10.2151/jmsj.79.771
Lu R, Dong B (2001) Westward extension of North Pacific subtropical high in summer. J Meteor Soc Japan Ser II 79:1229–1241. https://doi.org/10.2151/jmsj.79.1229
Lu R, Li Y, Dong B (2007) East Asian precipitation increase under the global warming. J Korean Meteorol Soc 43:267–272
Mao J, Sun Z, Wu G (2010) 20–50-day oscillation of summer Yangtze rainfall in response to intraseasonal variations in the subtropical high over the western North Pacific and South China Sea. Clim Dyn 34:747–761. https://doi.org/10.1007/s00382-009-0628-2
Menon S, Hansen J, Nazarenko L, Luo Y (2002) Climate effects of black carbon aerosols in China and India. Science 297:2250–2253. https://doi.org/10.1126/science.1075159
Ninomiya K, Murakami T (1987) The early summer rainy season (Baiu) over Japan. In: Chang CP, Krishnamurti TN (eds) Monsoon meteorology. Oxford Univ. Press, New York, pp 93–121
Pu Z, Xu L (2009) MODIS/Terra observed snow cover over Tibetan Plateau: distribution, variation and possible connection with the East Asian summer monsoon (EASM). Theor Appl Climatol 97:265–278. https://doi.org/10.1007/s00704-008-0074-9
Rodwell MJ, Hoskins BJ (1996) Monsoons and the dynamics of deserts. Quart J Roy Meteor Soc 122:1385–1404. https://doi.org/10.1002/qj.49712253408
Seo K-H, Son J-H, Lee S-E, Tomita T, Park H-S (2012) Mechanisms of an extraordinary East Asian summer monsoon event in July 2011. Geophys Res Lett 39:n/a–n/a. https://doi.org/10.1029/2011GL050378
Stan C, Xu L (2014) Climate simulations and projections with a super-parameterized climate. Env Mod Soft 60:134–152. https://doi.org/10.1016/j.envsoft.2014.06.013
Sun Y, Ding Y (2010) A projection of future changes in summer precipitation and monsoon in East Asia. Sci China Earth Sci 53:284–300. https://doi.org/10.1007/s11430-009-0123-y
Sun S, Ying M (1999) Subtropical high anomalies over the western Pacific and its relations to the Asian monsoon and SST anomaly. Adv Atmos Sci 16:559–568. https://doi.org/10.1007/s00376-999-0031-2
Tao S, Chen L (1987) A review of recent research on the East Asian monsoon in China. In: Chang CP, Krishnamurti TN (eds) Monsoon meteorology. Oxford Univ. Press, New York, pp 60–92
Wang Y, Li S, Luo D (2009) Seasonal response of Asian monsoon to the Atlantic multidecadal oscillation (AMOC). J Geophys Res 114:D02112. https://doi.org/10.1029/2008JD010929
Wang B, Xiang B, Lee J-Y (2013) Subtropical high predictability establishes a promising way for monsoon and tropical storm predictions. Proc Natl Acad Sci 110:2718–2722. https://doi.org/10.1073/pnas.1214626110
Xiang B, Wang B, Yu W, Xu S (2013) How can anomalous western North Pacific subtropical high intensify in late summer? Geophys Res Lett 40:2349–2354. https://doi.org/10.1002/grl.50431
Yang H, Sun S (2003) Longitudinal displacement of the subtropical high in the western Pacific in summer and its influence. Adv Atmos Sci 20:921–933. https://doi.org/10.1007/bf02915515
Yu L, Gao YQ, Wang HJ, Guo D, Li SL (2009) North meridional overturning circulation in an enhanced freshwater input simulation. Chin Sci Bull 54:4724–4732
Zhang Q, Tao S (1999) The study of the sudden northward jump of the subtropical high over the Western Pacific. Acta Meteor Sin 57:539–548
Zhang L, Wang B, Zeng Q (2009) Impact of the Madden–Julian oscillation on summer rainfall in Southeast China. J Clim 22:201–216. https://doi.org/10.1175/2008jcli1959.1
Zhang P, Liu Y, He B (2016) Impact of east Asian Summer monsoon heating on the interannual variation of the South Asian high. J Clim 29:159–173. https://doi.org/10.1175/JCLI-D-15-0118.1
Zhao M (2014) An investigation of the connections among convection, clouds, and climate sensitivity in a global climate model. J Clim 27:1845–1862. https://doi.org/10.1175/jcli-d-13-00145.1
Zhou T et al (2009) Why the Western Pacific subtropical high has extended westward since the late 1970s. J Clim 22:2199–2215. https://doi.org/10.1175/2008jcli2527.1